

Comparative Study of the Passivation of Al(111) by Molecular Oxygen and Water Vapor

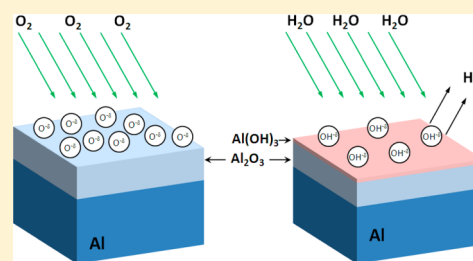
Na Cai and Guangwen Zhou*

Department of Mechanical Engineering & Multidisciplinary Program in Materials Science and Engineering, State University of New York, Binghamton, New York 13902, United States

Kathrin Müller[†] and David E. Starr[‡]

Center for Functional Nanomaterials, Brookhaven National Laboratory, Upton, New York 11973, United States

ABSTRACT: The self-limiting oxidation behavior of Al(111) surface by molecular oxygen and water vapor at room temperature is comparatively studied using X-ray photoelectron spectroscopy (XPS). The XPS Al(2p) and O(1s) core-level photoelectron lines are used to monitor the growth of the oxide passivation film, which showed that the limiting thickness increases with increasing gas pressure from 1×10^{-8} to 1×10^{-2} Torr. In comparison to oxide film growth via oxidation by molecular oxygen, the analysis of the Al(2p) and O(1s) peaks showed that oxidation by water vapor results in Al(OH)₃–Al₂O₃ bilayer film growth with a relatively constant thickness of the upper layer of Al(OH)₃. By fitting the experimentally measured passivation layer thicknesses, which depends on the oxidation time and gas pressure, with the logarithmic growth law from the Cabrera–Mott theory of metal oxidation, we find that oxidation with molecular oxygen results in a stronger Mott potential and thus a thicker limiting thickness of the oxide film than oxidation with water vapor. These results demonstrate that the passivation properties of a metal surface depend not only on the gas pressure but also on the type of oxidizing species used for the passivation.



1. INTRODUCTION

The interaction of gases with solid surfaces at low temperatures (e.g., room temperature) plays a crucial role in many technological applications such as corrosion, heterogeneous catalysis, and microelectronics. Oxygen and water vapor are perhaps the two most important oxidizing agents for gas–surface reactions. The interaction of water vapor with solid surfaces such as metal, semiconductor, and oxide surfaces has aroused a great interest due to the ubiquity of water. For instance, many heterogeneous catalytic reactions, such as Fischer–Tropsch synthesis of hydrocarbons, involve water as a reactant or product.^{1–4} Water moisture can cause distortions in electronic device characteristics.^{5–7} Furthermore, the corrosion of materials in humid environments is encountered in daily life and many studies pursue a fundamental understanding of corrosion and corrosion protection.^{8–10}

In ambient conditions, the reaction of aluminum (Al) surfaces with water vapor or oxygen results in a passivation layer. This makes Al an important material for applications where corrosion-resistance is required. The oxidation of Al at low temperatures leads to the formation of an amorphous Al oxide film.^{11–13} The amorphous oxides are particularly interesting for technological applications such as protective coatings, thermal barriers,^{14,15} and gate materials.^{16–18} For instance, the amorphous oxide films form relatively strain-free interfaces with the Al substrates due to the absence of epitaxial oxide growth and thermal strain that typically occurs for high-

temperature oxidation. Thus, many interfacial processes such as nonconformity and dewetting can be avoided. Also, the lack of grain boundaries in these films is desirable since grain boundaries are usually areas where corrosion is initiated.

The oxidation of Al using oxygen or an oxygen-containing atmosphere including water vapor has been studied extensively using a wide range of surface science techniques.^{19–31} In general, the oxidation of Al at low temperatures starts with a rapid initial oxidation stage followed by an abrupt reduction of the oxidation rate to virtually zero, when the limiting thickness of the oxide is reached. Since the growth of the oxide films at low temperatures does not allow for thermally activated diffusion processes, a classic model describing this self-limiting oxidation is the Cabrera–Mott model.^{32,33} According to this model, an electric field is formed across the oxide film. This field is a result of electron tunneling, which is driven by the potential difference (known as the Mott potential) between the Fermi level of the parent metal substrate and acceptor levels of chemisorbed oxygen at the surface. The self-generated electric field reduces the energy barrier for the migration of ions through the oxide film and makes oxide film growth possible at low temperature. As the tunneling current decreases with

Received: June 12, 2012

Revised: November 30, 2012

Published: December 11, 2012

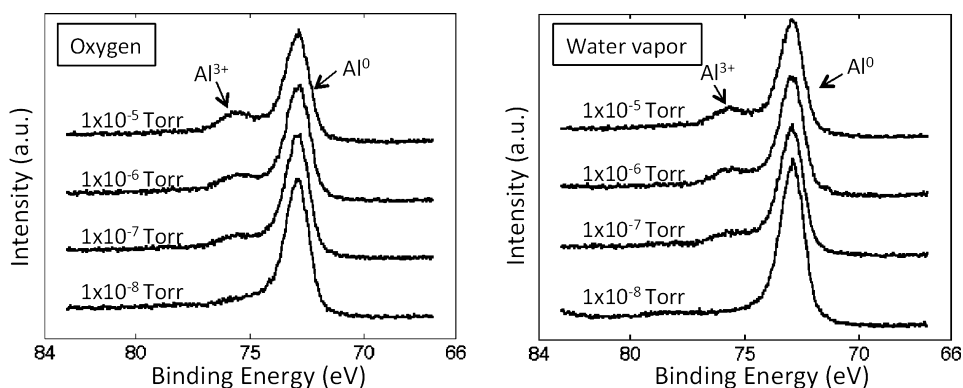


Figure 1. Photoemission spectra of the Al 2p core level region for extended exposures to molecular oxygen and water vapor at the indicated pressures.

increasing oxide film thickness, the oxidation virtually stops at a limiting thickness of the oxide film.

In an effort to understand the difference in the basic interactions of molecular oxygen and water vapor with Al leading to self-limiting oxide film growth at room temperature, we conducted a comparative study of the oxidation of Al(111) with the two oxidizing species, molecular oxygen and water. The oxidation kinetics and oxide film limiting thickness are measured for stepwise increases in gas pressure from 1×10^{-8} to 1×10^{-2} Torr. Practically, most gas–surface reactions (e.g., heterogeneous catalysis and oxidation) involve gas mixtures with different partial pressures for different gas species. Fundamental understanding of the reaction under these complex gas conditions is technically challenging due to the coupling of different processes. The way of carrying out oxidation experiments involving stepwise increases in gas pressure as shown here mimics the variations in gas partial pressure and the type of gas species and demonstrates in a clear way how the surface reactivity depends on the imposed environmental conditions. A number of key kinetic parameters including the Mott potential, rate-limiting ion diffusion barrier in the Al oxide films, and surface coverage of anions (oxygen and/or hydroxyl) are found to bear a strong dependence on the gas pressure and the type of oxidizing species. It is generally believed that the magnitude of the Mott potential is determined by the potential difference of the metal/oxide work function and the oxygen/oxide work function, without considering the effect of oxidation environmental conditions. This assumption is in contrast with our experimental results presented here, which reveal that the actual Mott potential created by the electronic species has strong dependence on the environmental conditions (i.e., gas pressure and oxidizing species). In addition, it is found that the oxidation of Al(111) surface by water vapor results in the bilayer growth of $\text{Al}(\text{OH})_3$ and Al_2O_3 in comparison of the single Al_2O_3 layer growth from the oxidation by molecular oxygen. Our results illustrate that molecular oxygen has stronger oxidizing power than water vapor owing to the larger Mott potential generated by oxygen surface adsorption, which leads to a larger limiting thickness of the oxide film. These observations also demonstrate that oxide film passivation of a metal surface depends on the environment in which it is used.

2. EXPERIMENTAL SECTION

The experiments were carried out in an ultrahigh vacuum chamber equipped with an X-ray photoelectron spectroscope

(XPS): SPECS Phoibos 100 electron energy analyzer and Ar-ion-gas sputtering gun. The chamber has a typical base pressure of 2×10^{-10} Torr. A nonmonochromatized Al-K α X-ray source ($h\nu = 1486.6$ eV) was used for the XPS studies. The Al(111) single crystal is a top-hat disk (1 mm thick and 8 mm in diameter), purchased from Princeton Scientific Corp., cut to within 0.1° to the (111) crystallographic orientation and polished to a mirror finish. The sample was heated via a ceramic button heater and its temperature monitored with a type-K thermocouple. The crystal was cleaned by cycles of Ar^+ sputtering (1×10^{-5} Torr of Ar^+ , $1 \mu\text{A cm}^{-2}$, 1.0 keV) followed by annealing at 420°C . The surface cleanliness was checked with XPS.

Oxygen gas (purity = 99.9999%) was directly introduced to the system through a variable pressure leak valve. Water ($18.2 \text{ M}\Omega$) was put into a glass flask (ACE) and further purified with several freeze–pump–thaw cycles before dosing through a variable pressure leak valve. The gas exposure was carried out at room temperature ($T = 25^\circ\text{C}$). An ion gauge was used to measure the gas pressure. The effect of the ion gauge sensitivity correction is not accounted during the pressure measurements due to the minor difference in the gas correction factors for O_2 and H_2O ($\text{O}_2 = 1.01$ and $\text{H}_2\text{O} = 1.12$ relative to $\text{N}_2 = 1.00$). For the initial stages of oxidation where no attenuation of the metallic Al^0 peak was detectable when the surface coverage by the oxide formed is less than 0.2 monolayers (ML), we first determined the oxide surface coverages by calculating the ratios of integrated O(1s) and oxidic $\text{Al}^{3+}(2p)$ peak areas with atomic sensitivity factors (ASF),³⁴ which were then converted into the average thickness of the oxide film by correlating with the Al_2O_3 monolayer thickness ($1 \text{ Al}_2\text{O}_3 \text{ ML} \approx 0.2 \text{ nm}$ ³⁵). For thicker and continuous oxide films formed from the higher gas exposures of molecular oxygen and water vapor, the film thicknesses are determined by the attenuation of the metallic Al(2p) XPS peak of the oxide films with the photoelectron attenuation length for Al_2O_3 ($\lambda = 16.7 \pm 0.6 \text{ \AA}$),^{36,37} by using the formula $d = -\lambda \cos \theta \ln(A/A_0)$, where A is the area of Al metallic peak after oxygen exposure, A_0 is the area of the Al metallic peak before oxygen exposure, λ is the inelastic mean free path, and θ is the angle between the analyzer and the sample surface normal, 0° in our case.³⁸ The sticking coefficients for the oxidation by O_2 and H_2O were also determined from the XPS measured oxidation kinetics.

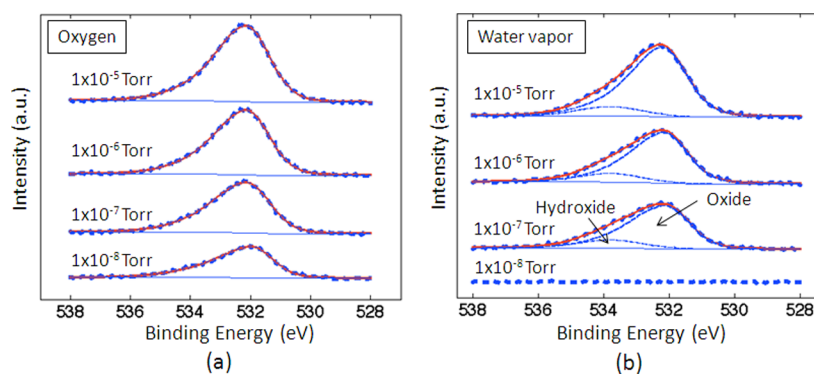


Figure 2. Photoemission spectra of the O(1s) region for extended exposures to molecular oxygen (a) and water vapor (b) at the indicated pressures. The O(1s) XPS spectra in panel b shows a peak that is broadened to the higher BE side and is deconvoluted into two peaks.

3. RESULTS

The freshly cleaned Al(111) is first exposed to molecular oxygen or water vapor at a pressure of 1×10^{-8} Torr. Figure 1a shows representative XPS spectra of the Al(2p) core level obtained from an Al(111) surface oxidized at increasing oxygen gas pressures. For oxidation with molecular oxygen, oxide film growth as a function of the oxygen exposure time results in the attenuation of the intensity of the Al(2p) metallic component (binding energy (BE) = 72.8 eV) and an increase of the Al(2p) oxide component (BE = 75.6 eV). Once no further changes in the peak intensities are detected, the oxygen pressure is then increased to 1×10^{-7} Torr, which results in an increase in the intensity of the oxidic Al(2p) peak and a further decrease in the intensity of the metallic Al(2p) peak. After reaching the saturation intensity of the peaks at this pressure, the oxygen pressure is then increased again and new saturated intensities of the two peaks are observed with prolonged oxygen exposure at the increased pressure.

Figure 1b shows XPS spectra of the Al(2p) peaks from Al(111) surface oxidized by water vapor at the different gas pressures. In contrast to oxidation with molecular oxygen, for water vapor exposure at $p(\text{H}_2\text{O}) = 1 \times 10^{-8}$ Torr, there is no detectable oxidic Al(2p) peak. Only when the pressure is increased to $p(\text{H}_2\text{O}) = 1 \times 10^{-7}$ Torr or higher does the oxidic Al(2p) peak becomes visible, which then increases in intensity with increasing water gas pressure. The position of the metallic Al(2p) peak position at the different pressures is constant at 72.8 eV, while its intensity decreases with increasing water vapor pressure above 1×10^{-7} Torr. These observations suggest a strong dependence of the limiting thickness of the passivation film on the gas pressure for both O_2 and H_2O .

Figure 2 shows photoemission spectra of the O(1s) peaks obtained from the limiting thickness oxide films on the Al(111) surface at the indicated pressures of oxygen and water vapor. Figure 2a corresponds to the O(1s) peak of the oxide film formed by the oxidation of molecular oxygen with a stepwise increase in oxygen gas pressure starting from $p(\text{O}_2) = 1 \times 10^{-8}$ to 1×10^{-5} Torr. The O(1s) peak at 532.3 eV is attributed to the oxygen in Al–O bonds in Al_2O_3 ,³⁹ and it can be seen that the saturated peak intensity increases with increasing oxygen gas pressure.

Figure 2b shows the obtained O(1s) XPS spectra from the Al surface oxidized by water vapor. For oxidation with water vapor, there is no detectable oxygen on the surface at the pressure of 1×10^{-8} Torr (as compared to the spectra obtained from the freshly cleaned Al surface). The O(1s) peak starts to become

visible only after the pressure is increased to 1×10^{-7} Torr and higher. In contrast to the O(1s) peak from oxidation with molecular oxygen (Figure 2a), the O(1s) spectra obtained from oxidation with water vapor show a broadening to high binding energy side. In our experiments, a mass spectrometer was used to monitor the gas composition. Tiny amounts of H_2O were present even for the molecular oxygen exposure at the gas pressure 1×10^{-8} Torr. However, their partial pressures were extremely low compared to the pressure of oxygen gas. As noted from the oxidation by water vapor, the Al surface was not oxidized for water vapor pressure at 1×10^{-8} Torr (Figure 2b). As such, it is reasonable to assume that the oxidation by molecular oxygen results in the formation of Al_2O_3 only. Therefore, the spectra as shown in Figure 2a were fitted with the oxidic O peak with the BE of 532.3 eV. However, using the same fitting parameters (e.g., fwhm, L–G%, and asymmetry of the oxidic peak from oxidation with the molecular oxygen) does not provide an overall good fitting to the O(1s) peak obtained from the Al surface being exposed to water vapor, and a second peak at the higher binding energy arises.

We have thus deconvoluted the spectra (i.e., shown in Figure 2b) into two peaks, with BEs of 532.3 and 533.8 eV. We have used the same fitting parameters for the 532.3 eV peak in both sets of data, which are the peak parameters obtained from fitting the data from oxidation with molecular oxygen alone. The peak at 532.3 eV is again attributed to oxygen in Al–O bonds of Al_2O_3 , and the other peak (BE = 533.8 eV) is attributed to oxygen in Al–OH bonds of aluminum hydroxide (i.e., $\text{Al}(\text{OH})_3$).^{40–43} It is clearly visible that the area under the Al–OH peak remains nearly constant, while the area under the Al–O peak curve increases with increasing water vapor pressure. This suggests that oxidation with water vapor occurs via Al_2O_3 layer growth to the limiting thickness, while the thickness of the $\text{Al}(\text{OH})_3$ layer remains relatively constant for the different gas pressures. The adsorption of water vapor on Al(111) at 25 °C is reported to be dissociative to form OH radicals on the surface.^{44–47} Thus, the reaction between the OH radicals and surface Al ions results in the formation of the outer layer of $\text{Al}(\text{OH})_3$. The growth of the inner Al_2O_3 layer occurs via the dehydration decomposition of the $\text{Al}(\text{OH})_3$ at the $\text{Al}(\text{OH})_3/\text{Al}_2\text{O}_3$ interface for the outward diffusion of Al^{3+} ions. This interfacial conversion mechanism of $\text{Al}(\text{OH})_3$ into Al_2O_3 is inferred from our experimental measurements on the thickness evolution of the $\text{Al}(\text{OH})_3$ and Al_2O_3 layers, which reveal that the $\text{Al}(\text{OH})_3$ layer has a relatively constant thickness, while the Al_2O_3 layer keeps growing with the continued H_2O vapor exposure. Such a behavior of the

thickness evolution suggests the interfacial conversion of $\text{Al}(\text{OH})_3$ into Al_2O_3 , otherwise there will be no Al_2O_3 formation due to the lack of O-species from the dissociation of H_2O , and the $\text{Al}(\text{OH})_3$ layer will keep thickening with the continued H_2O exposure.

Figure 3 shows the evolution of the passivation film thickness determined as described in the experimental section as a

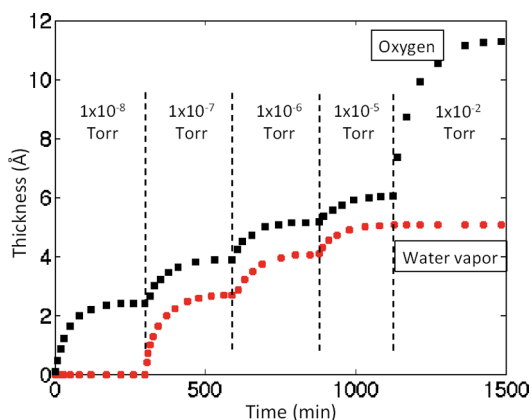


Figure 3. Evolution of the passivation film thickness for Al(111) oxidation as a function of oxidation time for molecular oxygen and water vapor. The oxidation starts with a clean Al surface, which is oxidized at 1×10^{-8} Torr. A stepwise increase in pressure is applied after a limiting passivation film thickness is reached at each pressure.

function of oxidation time and gas pressures. It can be seen that there is no passivation film growth for water vapor pressure of $p(\text{H}_2\text{O}) = 1 \times 10^{-8}$ Torr. In contrast, the Al oxide film starts to form with molecular oxygen at $p(\text{O}_2) = 1 \times 10^{-8}$ Torr. For both molecular oxygen and water vapor, the passivation films formed from the oxidation show an initial fast growth stage followed by a reduction in growth rate to the limited growth regime. After reaching the limiting passivation film thickness, a stepwise increase in the gas pressure is applied and a thicker limiting passivation film thickness is observed after long time exposure at this pressure. We also point out that this increase in the limiting thickness of the oxide film continues until a molecular oxygen pressure of $p(\text{O}_2) \approx 1$ Torr, beyond which the oxide film thickness remains essentially constant, irrespective of the prolonged molecular oxygen exposure and further increase in molecular oxygen pressure.^{48,49} Although the oxidation of Al(111) by water vapor also shows the stepwise growth of the limiting-thickness of the passivation film with the stepwise increases in water vapor pressure, we find here that the limiting-thickness increases in a stepwise manner only until a water vapor pressure of $p(\text{H}_2\text{O}) \approx 1 \times 10^{-5}$ Torr is reached, beyond which the passivation film thickness remains constant. We also found that the oxide film formed by stepwise increasing pressure has nearly the same limiting thicknesses of the oxide film on the Al surface that is immediately exposed to the highest pressure. This suggests that the pre-existing oxide film formed at a lower gas pressure has no effect on the subsequent oxide film growth at a higher gas pressure and that the self-limiting growth of the oxide film is determined by the gas pressure only for a constant oxidation temperature.⁴⁸

Extrapolating the data in Figure 3 to about 250 min, we derive the effective limiting passivation film thickness as the value of the thickness reached when the passivation film growth rate is less than 10^{-5} Å/s (i.e., less than one oxide ML per 10^5

s). Figure 4 shows the kinetic curves of the passivation film growth during the oxidation by molecular oxygen and water

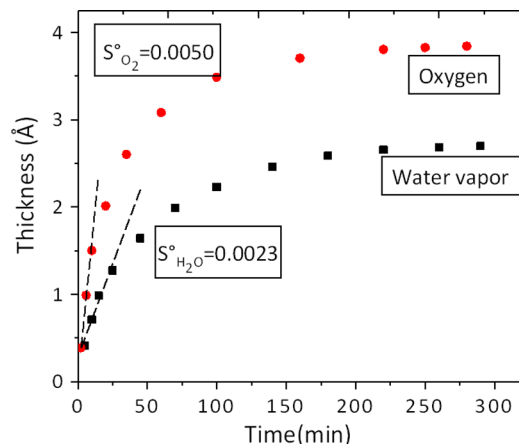


Figure 4. Kinetic growth curves measured with XPS over a time period extending to approximately 5 h for O_2 and H_2O at the gas pressure of 1×10^{-7} Torr. The initial sticking coefficient (estimated by the data at short time exposure, dotted line) of molecular oxygen is two times larger than that of water vapor.

vapor at the gas pressure of 1×10^{-7} Torr. It is obvious that the oxide film formed by oxidation with O_2 grows at a faster rate than that from oxidation with H_2O . The slopes of the initial linear portions of both curves are indicated and can be used to estimate the initial surface sticking coefficients depending on the gas exposure.⁵⁰ We find that surface sticking coefficients are $S^{\text{O}_2} = 0.005$ and $S^{\text{H}_2\text{O}} = 0.0023$, respectively, for O_2 and H_2O at the gas pressure of 1×10^{-7} Torr. The result of the sticking coefficient of molecular oxygen is comparable with earlier studies by Auger electron spectroscopy and scanning tunneling microscopy.⁵¹ The initial sticking coefficient for the O_2 oxidation is approximately 2 times higher than that for the H_2O exposure at this gas pressure. Similar differences in the surface sticking coefficients are found for the higher gas pressures.

As compared to the oxidation with molecular oxygen, a higher water vapor pressure is required to oxidize the Al surface. Experimentally, we were unable to determine the microscopic mechanism responsible for the abrupt increase in H_2O sticking probability across a decade of the gas pressure from 1×10^{-8} to 1×10^{-7} Torr, as shown in Figure 2b. Such abrupt increase in H_2O surface uptake by increasing the pressure from 1×10^{-8} to 1×10^{-7} Torr may suggest that the phase boundary for $\text{Al}(\text{OH})_3$ formation at room temperature is between the two pressures identified, and the significant adsorption at the water vapor pressure of 1×10^{-7} Torr could be driven by the thermodynamics of oxide formation.

4. DISCUSSION

The observed initially fast oxidation rate followed by a drastic reduction of the oxide film growth rate is consistent with the Cabrera–Mott theory of low-temperature oxidation of metals, which is characterized by a logarithmic growth law. The oxide growth can be controlled either by the outward diffusion of cations or inward diffusion of anions, depending on the type of vacancies in the oxide film. For the oxidation of Al, the oxide films formed at the relatively low temperatures ($T < 200$ °C) are amorphous in nature and can be described by a close

Table 1. Limiting Thickness of the Oxide Films, the Mott Potential V_M , Rate-Limiting Energy Barrier U for Cation Migration, and Anion Coverage Calculated from the Uptake Curves under Different Gas Pressures for the Oxidation by Molecular Oxygen and Water Vapor

pressure (Torr)	Oxygen				Water vapor			
	limiting oxide thickness (Å)	Mott potential V_M (V)	rate-limiting energy barrier U (eV)	oxygen anion coverage (Θ)	limiting oxide thickness (Å)	Mott potential V_M (V)	rate-limiting energy barrier U (eV)	anion coverage (Θ)
1×10^{-7}	3.81	0.1368	1.550	0.0383	2.70	0.0559	1.6431	0.0189
1×10^{-6}	5.14	0.3409	1.534	0.1262	4.07	0.1476	1.6444	0.0681
1×10^{-5}	5.99	0.6638	1.540	0.3064	5.04	0.3658	1.6421	0.1560

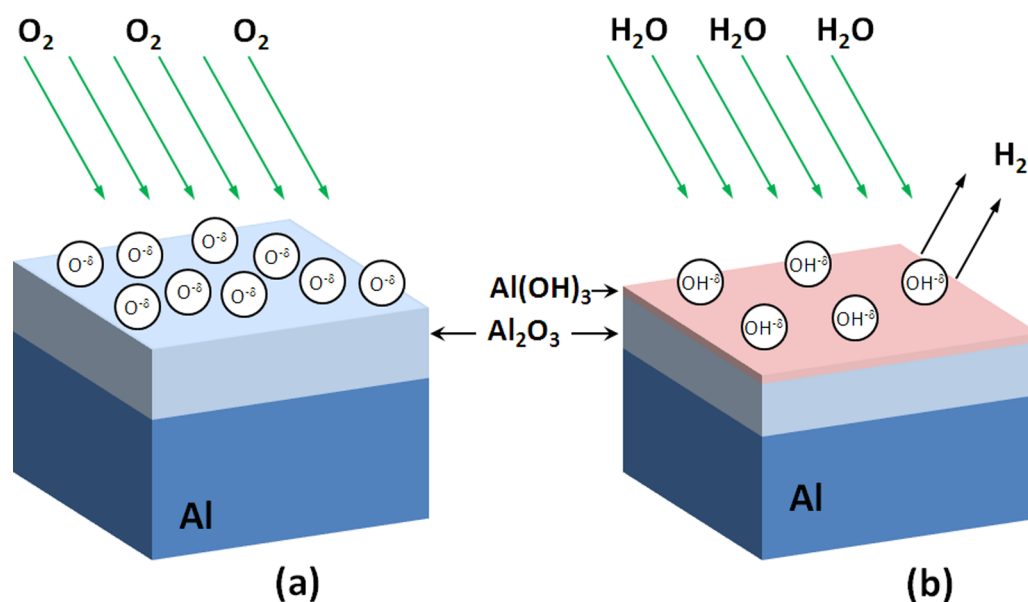


Figure 5. Schematic of the passivation oxide film growth during the oxidation of Al. (a) The oxidation of Al by molecular oxygen results in the growth of an Al_2O_3 thin film; (b) the oxidation of Al by water vapor leads to the growth of Al_2O_3 with $\text{Al}(\text{OH})_3$ on top, where the growth of the inner Al_2O_3 layer occurs via the decomposition of the top layer of $\text{Al}(\text{OH})_3$ into Al_2O_3 (δ denotes the charge state of adsorbed oxygen or hydroxyl group).

packing of oxygen anions with Al cations distributed over the octahedral and tetrahedral interstices and exhibit a deficiency of Al cations.^{52–56} This is also in line with our XPS measurements, where the stoichiometry of the oxide films formed with different oxygen gas pressures is approximately $\text{Al}_{(2-x)}\text{O}_3$ where $x \approx 0.24$, as determined from the Al/O peak intensity ratio.⁴⁸ Within this mechanism, the migration of cations under influence of the electric field $E = -V_M/X(t)$ from the Mott potential V_M is the rate-limiting step, where $X(t)$ is the oxide film thickness at the oxidation time t . By fitting the experimental data of the oxide film growth to the Cabrera–Mott inverse logarithmic law, the Mott potential V_M and the rate-limiting energy barrier U can be evaluated (details about this procedure are described in ref 48). The results are given in Table 1. It can be seen that the magnitude of the Mott potential V_M increases with increasing gas pressure for the oxidation by O_2 and H_2O ; however, the oxidation by O_2 shows a larger Mott potential than the oxidation by H_2O under the same gas pressure.

A parallel capacitor model can be employed to describe the development of the Mott potential induced by electron tunneling due to the potential difference between the acceptor level of chemisorbed species and the Fermi level of the Al substrate.^{48,49} According to the Langmuir isotherm for dissociative adsorption, the surface coverage of adsorbed species increases with increasing gas pressure. At a lower gas

pressure, there are fewer adsorbed species available for ionization by tunneling electrons, which results in a weaker electric field across the oxide film and thus a thinner limiting film due to the weaker driving force for ion migration and vice versa, as shown in Table 1.

The dissociative adsorption of water molecules results in chemisorbed hydroxyl radicals on the Al surface.²⁰ Hydroxyl radicals are electronegative and tend to form hydroxide anions. In the OH radical, the antibonding 1π orbital is partially vacant (i.e., there are unoccupied orbitals that are higher in energy).⁴⁶ Thus, the adsorbed hydroxyl radical is an electron acceptor and a net transfer of electrons from the metal surface to this partially vacant 1π orbital can occur. However, our observations indicate that, at the same pressure, the limiting thickness of the passivation film obtained by oxidation with water vapor is thinner than that by molecular oxygen. This suggests that the surface coverage of adsorbed OH^- anions formed via H_2O exposure is less than that of adsorbed O^- formed via O_2 exposure for the same gas pressure.

The surface density of adsorbed anions, N , on the oxide film surface can be determined using the capacitor-like model of the electric field established by the chemisorbed anions on the oxide surface and their counterpart Al cations at the metal/oxide interface. N is related to the Mott potential via $N = (V_M \epsilon_0 \kappa) / (X_L e)$, as given by Gauss' theorem for a field between the parallel plates, where ϵ_0 is the electric constant in vacuum, κ

is the relative permittivity and can be taken equal to $\kappa = 9.6$,⁵⁷ and X_L is the limiting thickness of the oxide film. The surface coverage, Θ , (using the density of Al in the Al(111) surface as the reference surface) of adsorbed anions for the different pressures are determined and given in Table 1. It is noted that the surface coverage of anions increases with increasing gas pressure for the oxidation by O_2 and H_2O .

Although the oxidation by O_2 and H_2O share a similar trend, i.e., the limiting passivation film thickness increases with increasing gas pressure, we find that the key kinetic parameters governing the oxide growth show different dependence on the gas pressure. As shown in Table 1, the Mott potential, the anion surface coverage, and the resulting limiting thickness of the oxide film formed by H_2O exposure are smaller than the ones for O_2 oxidation for the same gas pressure. The rate-limiting energy barrier U for ion migration is relatively constant despite the different gas pressures, but their values are different for the oxide films formed by oxidation with O_2 and H_2O , suggesting different microstructures and/or types of chemical bonding of the two types of the oxide films.

At the same gas pressure and oxidation temperature, the difference in the impingement fluxes due to the molecular weight difference between O_2 and H_2O is negligible for the prolonged exposure time involved in the current experiments. One O_2 molecule decomposes into two oxygen anions ($O_2 + 2e^- = 2O^-$), while one H_2O molecule decomposes into one hydroxyl radical and H_2 gas desorbed from the surface ($H_2O + e^- = OH^- + 1/2H_2$).²³ Obviously, one adsorbed H_2O molecule on the surface results in only one OH^- , while one adsorbed O_2 molecule results in two chemisorbed O^- available for accepting tunneling electrons. Therefore, for the same gas pressure, less adsorbed anions are available on the surface by water vapor compared with molecular oxygen, and thus, a smaller Mott potential is developed across the passivation film that leads to a thinner limiting thickness for water vapor. It should be noted that the model for dissociative adsorption of water on some oxide surfaces gives two hydroxyls for each water molecule.⁵⁸ One is formed from the addition of a proton (from water dissociation) to a surface oxygen atom and the other due to the attachment of the hydroxyl (from water dissociation) to a surface cation. The situation here for the water vapor oxidation is different though since the water is adsorbing onto a fully hydroxylated surface (i.e., $Al(OH)_3$).

Figure 5 shows a schematic comparison of the oxidation of Al by molecular oxygen and water vapor. On the basis of the O(1s) spectra in Figure 2, oxidation by water vapor results in the growth of a layer composed of Al_2O_3 , which is terminated by a layer containing hydroxyls groups similar to $Al(OH)_3$. On the basis of these results, the passivation film growth during the oxidation by water vapor can be described as follows. Water molecules dissociatively adsorb on the passivation film surface to form OH^- groups, and H_2 gas molecules desorb from the surface. Adsorbed OH^- groups are combined with exposed Al ions to form $Al(OH)_3$ on the outer surface via the hydration reaction, which is then converted into Al_2O_3 via dehydration reaction with H_2 desorbing from the surface. While the H_2 elimination processes as shown schematically in Figure 5 can be quite complex and too fast to detect by XPS, such a process of H_2 desorption for water vapor exposure is in line with previous studies.⁵⁸ The continued dissociative chemisorption of water molecules leads to the continuous $Al(OH)_3$ formation on the oxide surface, and the dehydration of $Al(OH)_3$ at the $Al(OH)_3/Al_2O_3$ interface via the outward diffusion of Al cations leads to

the growth of the Al_2O_3 layer. The dynamic balance between the hydration and dehydration processes of Al oxides results in the relatively constant thickness of the top $Al(OH)_3$ layer and therefore the observed constant O(1s) peak intensity at 533.8 eV. The larger rate-limiting energy barrier U (see Table 1) obtained from the oxidation by water vapor can be ascribed to such bilayer film growth, where the presence of the heterogeneous $Al(OH)_3/Al_2O_3$ interface can pose an additional energy barrier for ion transport. Other intermediate species such as $AlO_m(OH)_n$, which do not show up in the XPS due to their transient nature, may also form and contribute to the increased kinetic barrier during the H_2O passivation.

The passivating film growth described above also corroborates with the observed difference in the pressures at which the maximum thicknesses of the passivating layers are reached. As shown in Figure 3, the passivation layer formed by H_2O oxidation reaches its maximum thickness at the pressure of $p(H_2O) \approx 1 \times 10^{-5}$ Torr, beyond which the passivation film thickness remains constant, despite further exposure under higher H_2O pressures, while for the oxidation by molecular oxygen, the pressure of $p(O_2) \approx 1$ Torr is needed to reach such a maximum thickness of the passivation film.⁴⁸ For the oxidation by molecular oxygen, where the surface is terminated by Al_2O_3 , the surface density of Al cations is ~ 0.15 atoms/ \AA^2 (approximated using $\gamma'-Al_2O_3$ ^{59,60}). In comparison, the surface density of Al cations for the surface terminated by $Al(OH)_3$ from the oxidation by water vapor is 0.09 atoms/ \AA^2 (approximated using boehmite- $Al(OH)_3$ ⁶¹). Thus, the surface adsorption sites (the attachment of dissociated O or HO^-) to surface cations for the H_2O oxidation are less than that for O_2 oxidation, which results in a saturated coverage of the cation sites, and as a result, the maximum passivating film thickness, at a lower gas pressure for the oxidation by H_2O .

5. CONCLUSIONS

We report a comparative study of the oxidation of Al(111) with molecular oxygen and water vapor at room temperature by stepwise increases in gas pressure from 1×10^{-8} to 1×10^{-5} Torr. A logarithmic growth behavior of the oxide films appears with both gases consistent with the Cabrera–Mott theory for low temperature oxidation. However, molecular oxygen is a stronger oxidizing agent in terms of several key kinetic parameters including the resulting limiting thickness of the oxide film, the magnitude of the Mott potential, and the corresponding surface coverage of adsorbed anions. Our results demonstrate that self-limiting oxidation of the Al surface depends not only on the gas pressure but also on the type of the oxidizing agent.

■ AUTHOR INFORMATION

Corresponding Author

*E-mail: gzhou@binghamton.edu.

Present Addresses

†Zernike Institute for Advanced Materials, University of Groningen, Groningen, The Netherlands.

‡Helmholtz-Zentrum Berlin für Materialien und Energie GmbH, Institute Silicon-Photovoltaics, Kekuléstr. Five, 12489 Berlin, Germany.

Notes

The authors declare no competing financial interest.

■ ACKNOWLEDGMENTS

We acknowledge support from the National Science Foundation Grant No. CBET-0932814. Research was carried out in part at the Center for Functional Nanomaterials, Brookhaven National Laboratory, which is supported by the U.S. Department of Energy, Office of Basic Energy Sciences, under Contract No. DE-AC02-98CH10886.

■ REFERENCES

- (1) Li, K.; Fu, Q.; Flytzani-Slephanopoulos, M. *Appl. Catal., B* **2000**, *27*, 179–191.
- (2) Boccuzzi, F.; Chiorino, A.; Manzoli, M.; Andreeva, D.; Tabakova, T. *J. Catal.* **1999**, *188*, 176–185.
- (3) Hilaire, S.; Wang, X.; Luo, T.; Gorte, R. J.; Wagner, J. *Appl. Catal., A* **2001**, *215*, 271–278.
- (4) Liu, P. J. *Chem. Phys.* **2010**, *133*, 204705.
- (5) Hoshino, S.; Yoshida, M.; Uemura, S.; Kodzasa, T.; Takada, N.; Kamata, T.; Yase, K. *J. Appl. Phys.* **2004**, *95*, 5088–5093.
- (6) Comizzoli, R. B.; Frankenthal, R. P.; Milner, P. C.; Sinclair, J. D. *Science* **1986**, *234*, 340–345.
- (7) Lu, X.; Xu, G.; Hofstra, P. G.; Bajcar, R. C. *J. Polym. Sci., Part B: Polym. Phys.* **1998**, *36*, 2259–2265.
- (8) Sydyberger, T.; Vannerberg, N. G. *Corros. Sci.* **1972**, *12*, 775–784.
- (9) Oesch, S.; Faller, M. *Corros. Sci.* **1997**, *39*, 1505–1530.
- (10) Jeon, B.; Sankaranarayanan, S. K. R. S.; van Duin, A. C. T.; Ramanathan, S. *J. Chem. Phys.* **2011**, *134*, 234706.
- (11) Reichel, F.; Jeurgens, L. P. H.; Richter, G.; Mittemeijer, J. J. *Appl. Phys.* **2008**, *103*, 093515.
- (12) Doherty, P. E.; Davis, R. S. *J. Appl. Phys.* **1963**, *34*, 619–628.
- (13) Reichel, F.; Jeurgens, L. P. H.; Mittemeijer, E. J. *Acta Mater.* **2008**, *56*, 659–674.
- (14) Yin, Z. J.; Tao, S. Y.; Zhou, X. M. *Mater. Charact.* **2011**, *62*, 90–93.
- (15) Yun, S. J.; Ko, Y. W.; Lim, J. W. *Appl. Phys. Lett.* **2004**, *85*, 4896–4898.
- (16) Tahir, D.; Kwon, H. L.; Shin, H. C.; Oh, S. K.; Kang, H. J.; Heo, S.; Chung, J. G.; Lee, J. C.; Tougaard, S. *J. Phys. D: Appl. Phys.* **2010**, *43*, 255301.
- (17) Yoon, S. M.; Park, S. H. K.; Yang, S. H.; Byun, C. W.; Hwang, C. S. *Electrochem. Solid State Lett.* **2010**, *13*, H264–H267.
- (18) Yoon, S. M.; Yang, S. H.; Park, S. H. K.; Jung, S. W.; Cho, D. H.; Byun, C. W.; Kang, S. Y.; Hwang, C. S.; Yu, B. G. *J. Phys. D: Appl. Phys.* **2009**, *42*, 245101.
- (19) Popova, I.; Zhukov, V.; Yates, J. T. *Surf. Sci.* **2002**, *518*, 39–48.
- (20) Schmid, M.; Leonardelli, G.; Tscheliessnig, R.; Biedermann, A.; Varga, P. *Surf. Sci.* **2001**, *478*, L355–L362.
- (21) Popova, I.; Zhukov, V.; Yates, J. T. *Phys. Rev. Lett.* **2002**, *89*, 276101.
- (22) Zhukov, V.; Popova, I.; Yates, J. T. *J. Vac. Sci. Technol., A* **1999**, *17*, 1727–1732.
- (23) Paul, J.; Hoffmann, F. M. *J. Phys. Chem.* **1986**, *90*, 5321–5324.
- (24) Popova, I.; Zhukov, V.; Yates, J. T.; Chen, J. G. *J. Appl. Phys.* **1999**, *86*, 7156–7159.
- (25) Ebinger, H. D.; Yates, J. T. *Phys. Rev. B* **1998**, *57*, 1976–1984.
- (26) Ebinger, H. D.; Yates, J. T. *Surf. Sci.* **1998**, *412–413*, 1–14.
- (27) Do, T.; McIntyre, N. S. *Surf. Sci.* **1999**, *440*, 438–450.
- (28) Szalkowski, F. J. *J. Chem. Phys.* **1982**, *77*, 5224–5227.
- (29) Netzer, F. P.; Madey, T. E. *Surf. Sci. Lett.* **1983**, *127*, L102–L109.
- (30) Kurueger, W. H.; Pollack, S. R. *Surf. Sci.* **1972**, *30*, 280–298.
- (31) Fuggle, J. C.; Watson, L. M.; Fabian, D. J.; Affrossman, S. *Surf. Sci.* **1975**, *49*, 61–76.
- (32) Cabrera, N.; Mott, N. F. *Rep. Prog. Phys.* **1949**, *12*, 163–184.
- (33) Fromhold, A. T., Jr. *Fundamental Theory of Metal Oxidation*; North-Holland Publishing Company: Amsterdam, The Netherlands, 1976.
- (34) Wagner, C. D. *Surf. Interface Anal.* **1981**, *3*, 211–225.
- (35) Jeurgens, L. P. H.; Sloof, W. G.; Tichelaar, F. D.; Mittemeijer, E. *J. Phys. Rev. B* **2000**, *62*, 4707–4719.
- (36) Graupner, H.; Hammer, L.; Heinz, K.; Zehner, D. M. *Surf. Sci.* **1997**, *380*, 335–351.
- (37) Batty, F. L. *Phys. Rev. B* **1974**, *9*, 2887–2893.
- (38) Tanuma, S.; Powell, C. J.; Penn, D. R. *Surf. Interface Anal.* **1994**, *21*, 165–176.
- (39) Kishi, K.; Ikeda, S. *Bull. Chem. Soc. Jpn.* **1973**, *46*, 341–345.
- (40) Gao, Y. F.; Nagai, A.; Masuda, Y.; Sato, F.; Seo, W. S.; Koumoto, K. *Langmuir* **2006**, *22*, 3521–3527.
- (41) Otomo, S.; Hashizume, T.; Hasegawa, H. A Novel Thin Al₂O₃ Gate Dielectric by ECR-Plasma Oxidation of Al for AlGaIn/GaN Insulated Gate Heterostructure Field-Effect Transistors. *Proceedings of the International Workshop on Nitride Semiconductors* **2002**, 90–94.
- (42) Rotole, J. A.; Sherwood, P. M. A. *J. Vac. Sci. Technol., A* **1999**, *17*, 1091–1096.
- (43) Alvarez-Barcia, S.; Flores, J. R. *J. Chem. Phys.* **2011**, *134*, 244305.
- (44) Crowell, J. E.; Chen, J. G.; Hercules, D. M.; Yates, J. T. *J. Chem. Phys.* **1987**, *86*, 5804–5815.
- (45) Frederick, B. G.; Apai, G.; Rhodin, T. N. *Surf. Sci.* **1991**, *244*, 67–80.
- (46) Thiel, P. A.; Madey, T. E. *Surf. Sci. Rep.* **1987**, *7*, 211–385.
- (47) Swiatla-Wojcik, D.; Szala-Bilnik, J. *J. Chem. Phys.* **2012**, *136*, 064510.
- (48) Cai, N.; Zhou, G.; Müller, K.; Starr, D. E. *Phys. Rev. Lett.* **2001**, *107*, 035502.
- (49) Cai, N.; Zhou, G. W.; Muller, K.; Starr, D. E. *Phys. Rev. B* **2011**, *84*, 125445.
- (50) Zhukov, V.; Popova, I.; Yates, J. T. *Surf. Sci.* **1999**, *441*, 251–264.
- (51) Brune, H.; Wintterlin, J.; Trost, J.; Ertl, G.; Wiechers, J.; Behm, R. J. *J. Chem. Phys.* **1993**, *99*, 2128–2148.
- (52) Graat, P. C.; Somers, M. A. J.; Vredenberg, A. M.; Mittemeijer, E. J. *J. Appl. Phys.* **1997**, *82*, 1416–1422.
- (53) Snijders, P. C.; Jeurgens, L. P. H.; Sloof, W. G. *Surf. Sci.* **2002**, *496*, 97–109.
- (54) Jeurgens, L. P. H.; Sloof, W. G.; Tichelaar, F. D.; Mittemeijer, E. *J. Thin Solid Films* **2002**, *418*, 89–101.
- (55) Jeurgens, L. P. H.; Sloof, W. G.; Tichelaar, F. D.; Mittemeijer, E. *J. Surf. Sci.* **2002**, *506*, 313–332.
- (56) Hasnaoui, A.; Politano, O.; Salazar, J. M.; Aral, G. *Phys. Rev. B* **2006**, *73*, 035427.
- (57) Shamala, K. S.; Murthy, L. C. S.; Rao, K. N. *Mater. Sci. Eng., B* **2004**, *106*, 269–274.
- (58) Wang, G. C.; Tao, S. X.; Bu, X. H. *J. Catal.* **2006**, *244*, 10–16.
- (59) Reichel, F.; Jeurgens, L. P. H.; Richter, G.; van Aken, P. A.; Mittemeijer, E. J. *Acta Mater.* **2007**, *55*, 6027–6037.
- (60) Guo, J. X.; Guan, L.; Bian, F.; Zhao, Q. X.; Wang, Y. L.; Liu, B. T. *Surf. Interface Anal.* **2011**, *43*, 940–944.
- (61) Digne, M.; Sautet, P.; Raybaud, P.; Toulhoat, H.; Artacho, E. *J. Phys. Chem. B* **2002**, *106*, 5155–5162.